

VOLUMETRIC HELICAL ADDITIVE MANUFACTURING: SUPPLEMENTARY MATERIALS

LIGHT: ADVANCED MANUFACTURING

Antoine Boniface ¹, Florian Maître ¹, Jorge Madrid-Wolff ¹, Christophe Moser ^{1*}

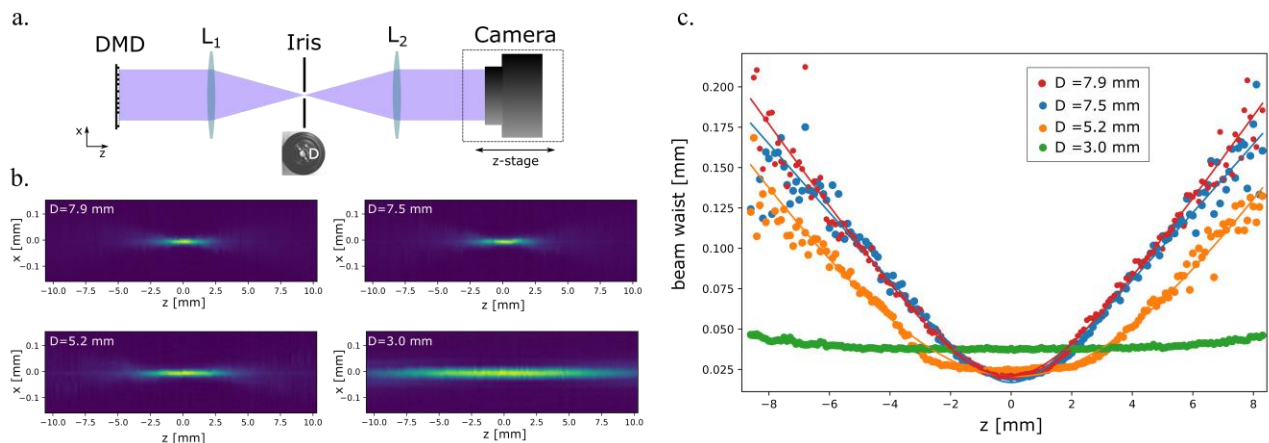
¹ Laboratory of Applied Photonics Devices, School of Engineering,
Ecole Polytechnique Fédérale de Lausanne, CH-1015 Lausanne,
Switzerland

*Correspondence to: christophe.moser@epfl.ch

2023

1 Characterization of the Beam Divergence

The divergence of a laser beam is a measure for how fast it expands apart from the imaging/focal plane. Note that it is not a local property of the beam, for a certain position along its path, but a property of the beam as a whole. An easy way to change the beam divergence is to change the numerical aperture of the optical system. In practice it consists of adjusting the diameter of an iris correctly placed in a Fourier plane (accessible at the focal plane of a lens prior to exciting the resin). Closing the iris results in elongating the beam along the optical axis, meaning reducing its divergence but it has a consequence: cutting off the high spatial frequencies of the beam affects not only the resolution at the focal plane but also the amount of light. For printing low beam divergence is essential especially for printing large objects, but the optical resolution and the overall light budget linked to the printing speed are also very important and a compromise has therefore to be found.

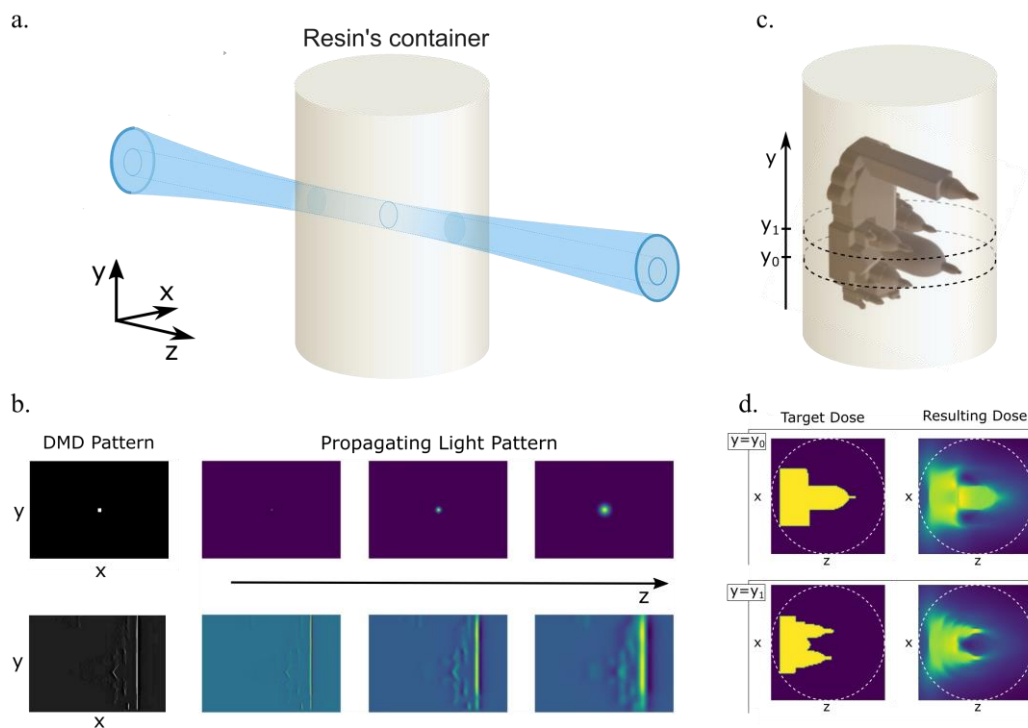


Supplementary figure 1. Effect of four different apertures on the beam divergence. **a.** Schematic of the optical setup used to characterize beam divergence. **b.** Point-spread-functions (PSF) for four different diameters of the iris D (see inset). **c.** Corresponding beam waist $w(z)$ as a function of z .

2 Beam Divergence simulation with a 3D Gaussian kernel

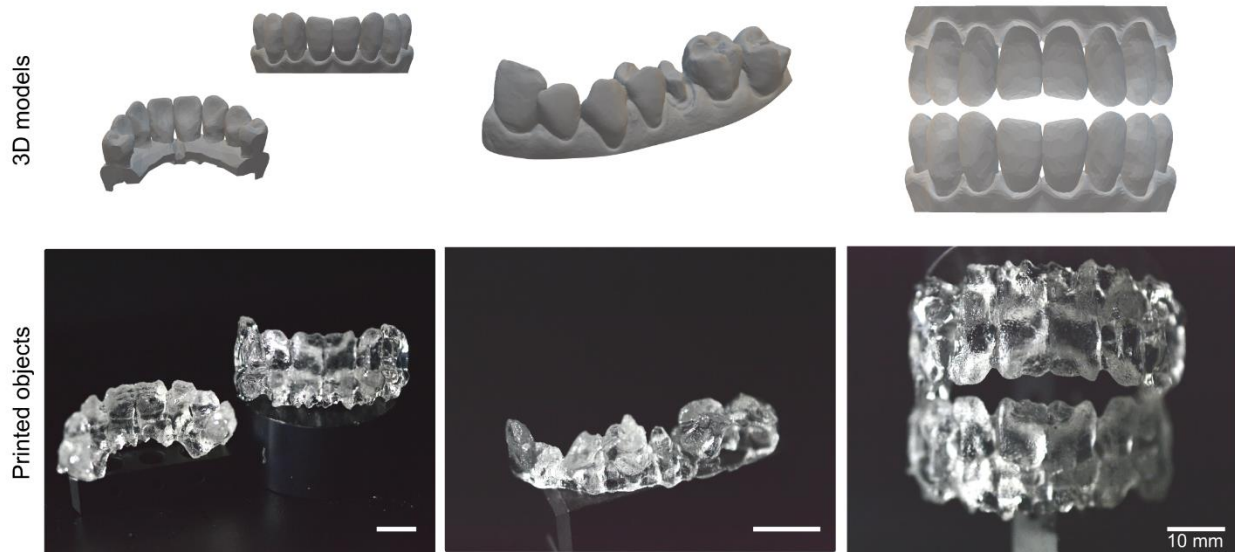
Most algorithms for tomography assume a perfectly collimated beam of light, but in practice this is not exactly the case because of light divergence. Assuming that light propagates in a homogeneous medium, some amount of divergence is unavoidable due to the general nature of waves. That amount is directly related to the numerical aperture of the optical system and is larger for tightly focused beams, corresponding to high NA. Light divergence is one of the factors that limits the resolution with which a 3D dose distribution can be projected inside the photosensitive material. To study this effect, we simulate the beam divergence in our Radon transform algorithm. Divergence is computationally implemented using a convolution with a 3D Gaussian Kernel. The parameters of the kernel are adjusted at different

depth in order to follow the theoretical trend of the beam width, $w(z) = w_0 \sqrt{1 + \left(\frac{z}{z_{Rayleigh}}\right)^2}$, where w_0 is the beam waist and $z_{Rayleigh}$ the Rayleigh length of the beam (Figure 3.b). This results in a global loss of fidelity, as seen in Figure 4.d. We can also see that it is responsible for a non-homogeneous printing resolution; the voxel size is increasingly larger when moving further away from the imaging plane (middle of the cylindrical vial).



Supplementary figure 2: Simulation of a tomographic printer with a divergent beam.

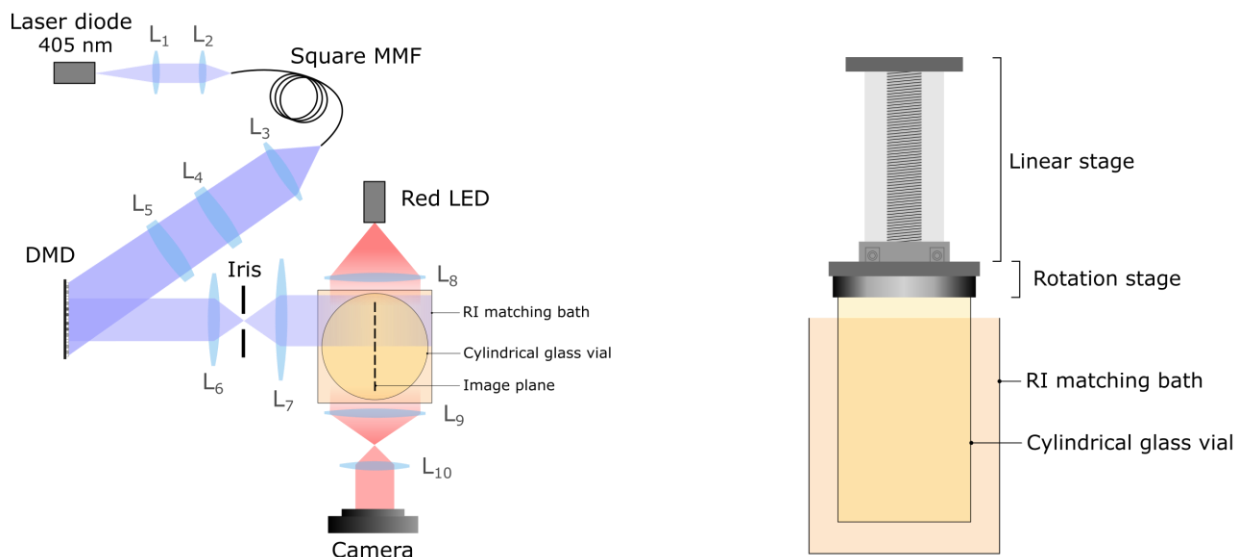
3 Fabrication of dental models



Supplementary figure 3. High-resolution printing of adult-size teeth. Scalebars: 10 mm.

We explored the possibility of fabricating adult dental models (freely available online) on clear acrylate resins. The models were printed in 6 minutes and less, which is a very competitive manufacturing time. However, print fidelity can still be improved. A major challenge was making sure that light dose was not excessive, so that negative features (like spaces between teeth) were present, but not too low so that all positive features were present. Gums, which were at the extreme of the prints and exhibited both positive and negative features, were challenging to fabricate and are missing in several of the prints.

4 Optical Setup

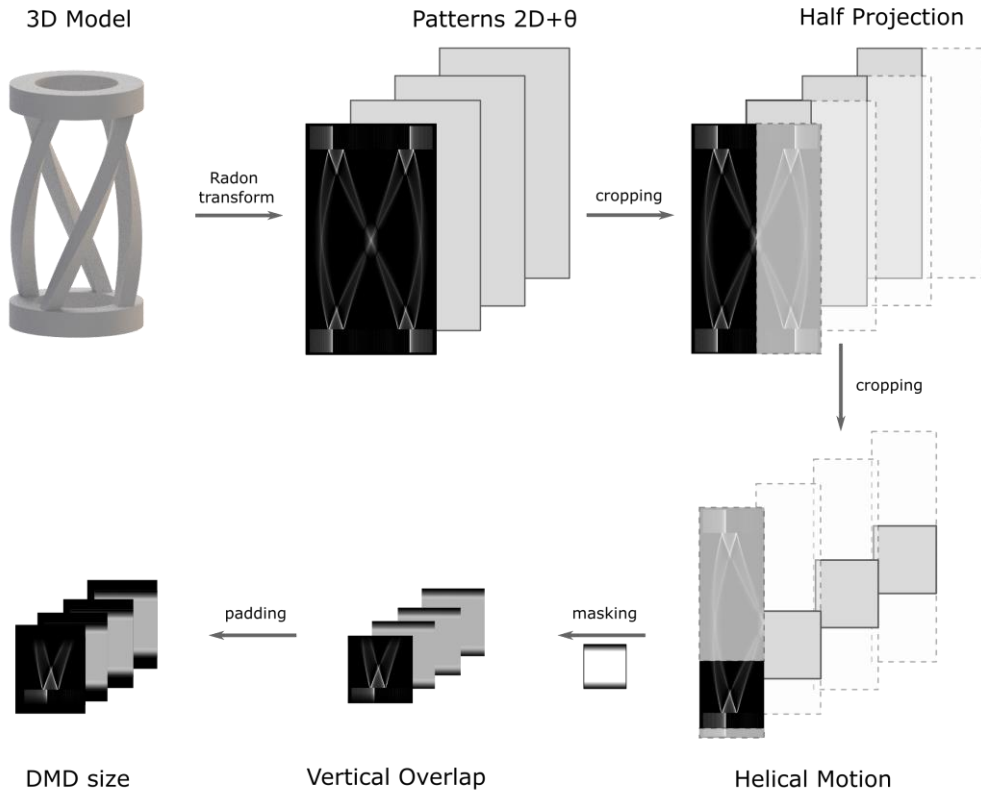


Supp. fig. 4 Experimental setup. L₁: f = 4.02 mm aspheric lens ; L₂: f = 11 mm aspheric lens; Square MMF: 70 μ m by 70 μ m square-core optical fiber; L₃: f = 2 mm aspheric lens; L₄: f = 250 mm cylindrical lens; L₅ : f = 300 mm cylindrical lens; DMD: digital micromirror device (Vialux V-7000 VIS); L₆: f = 150 mm lens; A: variable aperture; L₇: f = 250 mm lens; cylindrical glass vial: outer diameter 32 mm, wall thickness 1 mm; L₈: f = 40 mm lens; L₉: f = 250 mm lens; L₁₀: f = 35 mm lens; camera: DCC3260C USB 3.0 CMOS Camera, Thorlabs; Linear stage: LSQ075A, Zaber; Rotation stage: X-RSW60C, Zaber.

The optical setup for tomographic VHAM is presented in Figure S1. Two 405 nm laser diodes, with a combined nominal power of 1.8 W, are collimated and combined into a single beam with a closely spaced mirror. The combined beam is then coupled into a square-core optical fiber (CeramOptec WF 70x70/115/200/400N, core size 70 μ m by 70 μ m, numerical aperture 0.22), in order to spatially homogenize the beam from the two laser diodes. The outgoing square beam is then magnified to match the rectangular aperture of the digital micromirror device (DMD) via an aspheric lens L₃ and a set of two orthogonal cylindrical lenses L₄ and L₅ for maximizing the light efficiency. Note that the cylindrical lenses have different focal lengths ($f_4 = 250$ mm and $f_5 = 300$ mm), in order to adjust the square beam from the fiber square output facet to the rectangular area of the DMD. The DMD suffers from diffractive effects due to the blazed

grating formed by the micromirrors (pitch = 13.6 μ m). This effect can cause a large fraction of the reflected light to be lost in diffracted orders depending on the incidence angle of the illumination beam. The surface of the DMD is imaged via a 4f-system into a cylindrical glass vial containing the photopolymer. In the Fourier plane (between L₆ and L₇), an iris blocks the unwanted diffraction orders from the DMD. A refractive index matching is used to remove the lensing distortion caused by the cylindrical interface of the vial. Compared to conventional tomographic VAM, the DMD is off-centered with respect to the vial's rotation axis and the resin can be moved vertically thanks to a linear stage (travel range of 10 cm). A side view camera placed perpendicular to the optical axis monitors the printing process. A red LED that does not influence the photopolymerization is used for this purpose.

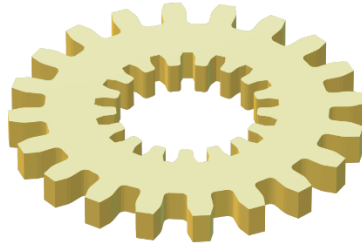
5 Light Patterns Computation



Supp. Fig. 5: Workflow for computing the light patterns

The computation of the light patterns from the target dose relies essentially on the Radon transform as developed for tomographic imaging. However, in the case of printing, the problem to solve is reversed: one has to compute the 2D patterns from the 3D dose whereas in imaging the algorithm aims at reconstructing the 3D object from a set of 2D measurement [1]. As in tomographic VAM [2], [3], the starting point is the 3D model, i.e. the object one intends to print. The latter is first voxelized into a three-dimensional binary matrix, where the entries “1” indicate the presence of matter and “0” its absence at each particular location in space. The voxel size depends on the optical setup and is in our case around 23 μm . The dimension of the matrix is therefore given by the target object size divided by the voxel size. This matrix also represents the normalized target dose that one would need to deposit in a transparent resin to polymerize it in the desired geometry. A series of dose projections over multiple angles are calculated from the Radon transform. More precisely, the patterns are obtained using a filtered back-projection algorithm followed by an optimization subject to positivity constraint. Please note that this forward model assumes the use of optically-clear materials, in which light propagates straight and without attenuation. The obtained patterns are too large to be entirely projected with the DMD. For these reasons they are cropped twice. First, along the horizontal axis, because the DMD is off-centered and second vertically to account for the up and down moving of the vial. These two crops allows for reducing the image size to a pattern that can be projected onto the DMD. To avoid any printing discontinuity along the vertical direction the patterns are softened on the correspond edges over with a smoothing mask that contains overlap region of adjustable height. The last step consists of padding with zeros the patterns to fit the DMD size.

6. Resolution target



Sup. Fig. 6: Resolution target. A double-sided gear with a non-matching number of cogs in the outside and the inside is used as a resolution target.

Features	Xolography	CAL		Tomographic VAM	Helical VAM
DLP chip ($N_x \times N_y$ px)	3840×2160 px	912×1140 px	2716×1528 px	1024×768 px	1024×768 px
Image pixel pitch	$21 \mu\text{m} \times 21 \mu\text{m}$	$38 \mu\text{m} \times 38 \mu\text{m}$	$31 \mu\text{m} \times 31 \mu\text{m}$	$23 \mu\text{m} \times 23 \mu\text{m}$	$23 \mu\text{m} \times 23 \mu\text{m}$
Number of voxels	$N_x \times N_y \times N_z$	$\frac{\pi}{4} N_x^2 \times N_y$	$\frac{\pi}{4} N_x^2 \times N_y$	$\frac{\pi}{4} N_x^2 \times N_y$	$4\alpha \frac{\pi}{4} N_x^2 \times N_y$
ON pixel intensity	215 mW.cm^{-2}	8.7 mW.cm^{-2}	10.5 mW.cm^{-2}	400 mW.cm^{-2}	70 mW.cm^{-2}
Print resolution corresp. object's size	$\sim 80 \mu\text{m}$ $0.9 \text{ cm} \times 0.9 \text{ cm} \times 0.9 \text{ cm}$	$\sim 300 \mu\text{m}$ $1 \text{ cm} \times 1 \text{ cm} \times 1 \text{ cm}$	-	$\sim 80 \mu\text{m}$ $1 \text{ cm} \times 1 \text{ cm} \times 1.3 \text{ cm}$	$\sim 200 \mu\text{m}$ $2.5 \text{ cm} \times 2.5 \text{ cm} \times 3 \text{ cm}$
Max. dimensions	$3 \text{ cm} \times 3 \text{ cm} \times 4 \text{ cm}$	$4 \text{ cm} \times 4 \text{ cm} \times 4 \text{ cm}$	$2 \text{ cm} \times 2 \text{ cm} \times 2.7 \text{ cm}$	$1.7 \text{ cm} \times 1.7 \text{ cm} \times 2.3 \text{ cm}$	$3 \text{ cm} \times 3 \text{ cm} \times 6 \text{ cm}$
Print time	1-8 min	30-120 s	150 s	30-120 s	5-10 min
Print speed	$55 \text{ mm}^3.\text{s}^{-1}$	-	-	$30 \text{ mm}^3.\text{s}^{-1}$	$75 \text{ mm}^3.\text{s}^{-1}$

Sup. Table 1. Comparison of multiple volumetric additive manufacturing strategies.

References

- [1] N. U. Dinc *et al.*, “From 3D to 2D and back again,” *Nanophotonics*, Jan. 2023, doi: 10.1515/nanoph-2022-0512.
- [2] B. E. Kelly, I. Bhattacharya, H. Heidari, M. Shusteff, C. M. Spadaccini, and H. K. Taylor, “Volumetric additive manufacturing via tomographic reconstruction,” *Science*, vol. 363, no. 6431, pp. 1075–1079, 2019.
- [3] D. Loterie, P. Delrot, and C. Moser, “Volumetric 3D printing of elastomers by tomographic back-projection,” *Preprint at https://doi.org/10.13140/RG*, vol. 2, no. 20027.46889, 2018.